AIAA JOURNAL
Vol. 35, No. 6, June 1997

Experimental Demonstration of Use of N_2O to Increase Shock Tunnel Test Time

David W. Bogdanoff*
NASA Ames Research Center, Moffett Field, California 94035-1000
Gregory J. Wilson†
Semitool, Kalispell, Montana 59901
and
Myles A. Sussman‡
Parametric Technology Corporation, San Jose, California 95131

An experimental investigation was carried out into the replacement of air in the driven tube of a reflected shock tunnel by an N_2O/N_2 mixture in order to increase the test time. The final gas mixture obtained is the same with either air or N_2O/N_2 in the driven tube. The incident shock velocities were between 2 and 3 km/s. Test times (or times until driver gas arrival) were estimated from light emission histories in the driven tube and in the nozzle and from pressure histories just upstream of the nozzle entrance. The test times estimated from the light emission histories behind the incident shock showed that consistent increases of 60–100% were obtained upon substituting N_2O/N_2 for air in the driven tube. These increases were in good agreement with theoretical estimates. The test times estimated from the light emission histories in the nozzle or pressure histories at the nozzle inlet showed significant improvements with N_2O/N_2 only for cases where the facility was operated at substantially overtailored conditions, probably due to the greater stability of the driver–driven interface at these conditions. At overtailored operating conditions, test times increases of 60–100% with N_2O/N_2 were observed with all three diagnostic techniques. These increases were in reasonable agreement with theoretical estimates.

Nomenclature

$H5$	= enthalpy after shock reflection
P	= plateau region
$P0.4$, $P1.7$, etc.	= plateau duration in multiples of 100 μs
$P1$	= initial fill pressure in driven tube
$P5$	= pressure after shock reflection
PR	= pressure rise region
R_h	= ratio of assumed static enthalpy to that which would be obtained by simple constant pressure mixing of driver and driven gases
u_{BC}, u_{CD}, u_{DE}	= shock velocities calculated between the two data stations denoted by the subscripts
u_E	= shock velocity extrapolated to station E
V	= valley region
x	= axial coordinate along driven tube
x_{mn}, x_{mr}	= axial locations of boundaries between mixed driver/driven gas and pure driven or driver gas, respectively
γ	= specific heat ratio
ρ	= gas density

I. Introduction

REFLECTED shock tunnels[1–10] are very important ground test facilities for flight Mach numbers from 8 to 16. Test times in these facilities are typically short, 0.5–10 ms being representative, and are only about $\frac{1}{3}$–$\frac{1}{2}$ of the theoretical values. The short test times impose limits on the amount of data that can be obtained and the size of the test article and make it more difficult to ensure that the flow is established over the test article before the acquisition of steady-state data. As the nozzle plenum total enthalpy increases, the available test time decreases sharply and can become too short to gather reliable data. The test time can be increased by increasing the size of the facility, but large facilities are very expensive to build and operate.

For tests with air as the working gas, significant (30–100%) increases in test time can be achieved by replacing air in the driven tube by a mixture of $2N_2O + 1.76N_2$. By varying the initial driven tube fill pressures and the shock velocities, the same final, high-temperature test gas can be obtained whether one starts with air or $2N_2O + 1.76N_2$ in the driven tube. The increase in test time is due largely to the chemical energy release occurring behind the incident or reflected shock wave, which results in a substantially decreased volumetric compression across the wave in which the energy is released. This technique is simple, inexpensive, and can be applied to any facility. The safety hazards of nitrous oxide appear to be minor: certainly no greater than those of hydrogen, which is commonly used in the driver gas of hypersonic shock tunnels.[11] The advantages of the technique would be 1) increasing the useful enthalpy range of the facility, inasmuch as higher enthalpy levels would be obtainable with acceptable test times; 2) obtaining more data and having greater confidence that a flow was established over the test article before steady-state data were taken; and 3) testing of larger test articles would be possible.

A computational analysis of the use of N_2O/N_2 mixtures as the driven tube gas in reflected shock tunnels was presented in Ref. 11. A model assuming an inviscid, one-dimensional flow with finite-rate chemistry was used. The chemistry model included 8 species (N_2O, N_2, O_2, NO, N, O, NO_2, and He) and 12 elementary reactions. The numerical algorithm used is based on one that has been validated using experimental data from a number of high enthalpy facilities (shock tubes, shock tunnels, and expansion tubes).[11,12] The results of this theoretical study predicted that by substituting N_2O/N_2 for air in the driven tube of a shock tube, the test gas volume can be increased 100% at a nozzle plenum enthalpy of 5.5 MJ/kg. This increase falls to 50% at an enthalpy of 9 MJ/kg and to 30% at an enthalpy of 14 MJ/kg.

An important early (1967) experimental demonstration of the use of N_2O/N_2 in the driven tube of a shock tube was carried out by

Received Nov. 12, 1996; revision received March 14, 1997; accepted for publication March 17, 1997.

*Senior Research Scientist, Thermosciences Institute. Associate Fellow AIAA.
†Staff Engineer, Thermal Products Division. Member AIAA.
‡Member of the Technical Staff, Analysis Technology/Mechanica Division.

Craig and Ortwerth.[13] This work was limited to enthalpies below 5 MJ/kg and was aimed toward the experimental demonstration of increases in enthalpy and pressure rather than toward increases in test time. This work was very successful in demonstrating experimentally the desired increases in enthalpy and pressure, and the results were also used by the authors of Ref. 11 to help validate their computational methods.

II. Facility and Test Conditions

The experiments were carried out in the electric arc-driven shock tube (EAST) at the NASA Ames Research Center. This facility is a 10.16-cm-diam shock tube with an electric arc-heated driver. Figure 1 shows a sketch of the facility. The arc in the driver is supported by a capacitor bank, which can store up to 1.24 MJ of energy at 40 kV. The driver gas is usually hydrogen, helium, or helium/argon mixtures. Reflected shock pressures up to 50 MPa can be obtained. Shock velocities ranging from 1.5 to 50 km/s have been obtained. Further description of the facility is given in Refs. 14 and 15.

For the present experiments, the facility was configured as follows. The driver and driven tube lengths were 76.2 and 548.95 cm, respectively. Table 1 gives these and other important axial locations in the facility configuration used. (Axial locations or x coordinates are measured from the primary diaphragm in the direction of the tube axis toward the driven tube.) The nozzle throat diameter is 1.588 cm, and the nozzle expands to an exit diameter of 10.16 cm at a distance 29.72 cm downstream from the driven tube end wall. The diagnostic ports F are located in a convenient flange 3.95 cm upstream of the nozzle exit, where the nozzle diameter is 8.382 cm. Because the ports are located at 87% of the distance between the driven tube end wall and the nozzle exit, the time of arrival of driver gas contamination at the ports F should be reasonably representative of that to be expected at the nozzle exit. The divergent part of the nozzle is a 10-deg half-angle cone. A 1.588-cm-diam square-faced rod is introduced into the nozzle along the centerline from the exit. The front of the rod is located at the center of the diagnostic ports F to allow light emission from the hot gas cap behind the bow shock to be observed.

Table 2 gives the operating conditions for the facility. In total, 29 runs were made over a period of six weeks. Conditions for similar runs have been grouped in Table 2. The data are run number, capacitance and initial voltage on capacitor bank, driver gas argon percentage (balance of driver gas is helium), driver gas fill pressure, nominal main diaphragm rupture pressure, driven tube gas composition (N_2O/N_2 denotes a mixture of $2N_2O + 1.76N_2$), driven tube gas fill pressure, and shock velocity measured between stations D and E. The error band of these shock velocities varies from $\pm$1.0 to $\pm$1.4% as the shock velocity increases from 2.0 to 2.8 km/s. Errors in shock velocities will be further discussed in Sec. IV.B.

Table 1 Key axial locations in the EAST facility

Location	x Coordinate, cm
Driver blind end	−76.20
Diaphragm	0.0
Diagnostic ports A	not used
Diagnostic ports B	187.64
Diagnostic ports C	340.99
Diagnostic ports D	462.92
Diagnostic ports E	546.41
Driven tube endwall	548.95
Diagnostic ports F	574.72

The main diaphragms (between the driver and driven gases) were scored and were made of 304 stainless steel for runs 1–18 and of 2024-0 aluminum for runs 20–29. For most of the test entry (runs 5–29), the secondary diaphragms (located at the nozzle entrance) were made of 0.0025-cm-thick Kapton® polyimide film.

III. Instrumentation

Facility pressures measured before each test included the driver fill pressure, the driven tube fill pressure, and the dump tank vacuum pressure. The portion of the facility downstream of the nozzle exit was pumped to a vacuum of about 0.7 Pa prior to each run. The voltage on the capacitor bank was measured before and after the discharge. An oscilloscope trace of the capacitor bank discharge current history was also obtained for each run. The configuration of instrumentation in the driven tube and nozzle are given in Table 3. The ion gauge consists of two 0.13-cm-diam wire electrodes, which protrude 0.05 cm into the flow. Because the next diagnostic station is 120 cm (or 2400 electrode protrusion lengths) downstream of the ion guage, the effect of the ion guage on the flow at the next diagnostic station should be completely negligible. A voltage of 50 V is applied across the electrodes and, upon arrival of the incident shock wave, the sudden conduction of electric current through the shock-heated gas produces a very abrupt voltage change at the ion gauge output that yields a very precise time for the passage of the shock. PCB 111A22 and PCB 113A24 are the model numbers of quartz crystal piezoelectric pressure transducers made by the PCB Corporation.

PMT 1P28 refers to type 1P28 photomultiplier tubes. These tubes viewed the shock tube flow through two slits of width 0.005–0.0125 cm oriented perpendicular to the direction of shock motion. The slits were separated by distances of 7.5–15 cm and are mounted in a small tube, which is placed just outside an acrylic window in the wall of the driven tube. MONO refers to a monochromator. The monochromator used is a Bausch and Lomb instrument with input and output slits 500 or 750 μm wide and 1.1 cm high. The distances from the slits to the mirror are 25 cm, and those from the mirror to the grating are 21 cm. The mirror diameter is 9.4 cm, and the grating is square, 5 cm on a side. The hot-gas cap in front of the rod inserted into the nozzle was imaged on the input slit at unity magnification with a lens of 100-cm focal length. An RG 610 long pass filter is used in front of the input slit. In the first 10 runs, the monochromator was operated at zeroth order and, thus, sensed broadband light emission. Thereafter, the monochromator was tuned to the argon 697-nm line in first order.

The arrows in the table (for ports E and F) indicate that the instrumentation at that particular diagnostic port was changed as the test series proceeded. The high-quality data indicating substantial increases in test time with operation of the facility in a overtailored mode were obtained mainly with the final instrumentation configuration, that is, the last configuration indicated in Table 3 for the ports at E and F. The signals from the diagnostics were digitized and recorded using 12 high-speed digitizers made by the DSP Corporation.

IV. Results

A. Preliminary Discussion

In the very short facility entry available for the present investigation, we were unable to develop and bring on-line a definitive

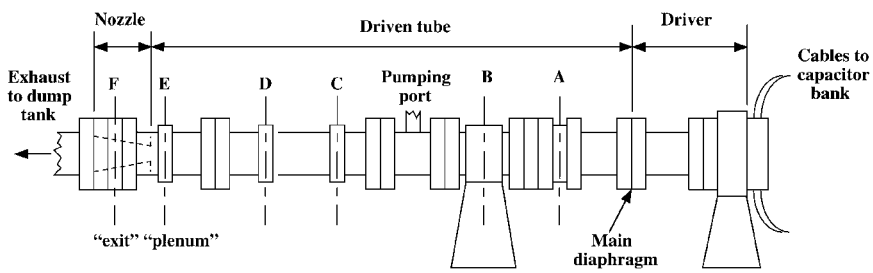

Fig. 1 NASA Ames Research Center EAST facility setup, not to scale: stations A–F each have two instrumentation ports available.

Table 2 Operating conditions for the EAST facility

Run	Driver: Capacitance, μF	Driver: Voltage, kV	Driver: Gas	Driver: Fill pressure, MPa	Diaphragm break pressure, MPa	Driven gas	Driven gas fill pressure, kPa	Shock velocity DE, km/s
1–6	1530	27.5	50Ar	2.90	17–37.4	Air	56–69.3	2.06–2.32
7–9	1530	27.5	50Ar	2.90	37.4–53.1	N_2O/N_2	89.7	2.00–2.13
10–14	1530	24.2	33Ar	2.90	37.4	Air	30.0	2.36–2.82
15,16	1530	24,25	33Ar	2.90	37.4	N_2O/N_2	40.4	2.46–2.61
17	1530	27.5	50Ar	2.90	37.4	Air	16.8	2.90
18	1530	27.5	50Ar	2.90	37.4	N_2O/N_2	20.8	2.73
19	——	——	All	data	lost	——	——	——
20–22	861.3	19–22	9–22Ar	2.24	2.59	Air	7.74	2.63–2.98
23, 24	861.3	22	33Ar	2.24	2.59	Air	7.74	2.71–2.73
25–28	861.3	22	33Ar	2.24	2.59	N_2O/N_2	7.74–11.5	2.40–2.61
29	861.3	22	33Ar	2.24	2.59	Ar	7.74	2.54

Table 3 Instrumentation in driven tube and nozzle

Diagnostic port station	Instrumentation	Instrumentation
B	Ion gauge	
C	PMT 1P28	PCB 113A24
D	PMT 1P28	PCB 113A24
E	PCB 111A22 > PMT 1P28 > PCB 111A22 > PCB 113A24	PCB 111A22
F	PCB 113A24 > PMT 1P28	MONO at zeroth order > MONO at Ar 697-nm line

spectroscopic technique to determine the time of arrival of the driver gas contamination, which determines the end of the useful test time. However, it was observed that, in the driven tube and the nozzle, a large, well-defined and consistent increase in light emission occurred in the time interval where the initial arrival of driver gas is expected. No other such increase was observed anywhere near the time interval in question. Such an increase in light emission upon driver gas arrival is to be expected, inasmuch as the driven gas is very clean, but the driver gas is contaminated by the vaporized driver trigger wire material and material ablated from the rubber lining of the fiberglass driver liner.[14] The times of the increases in light emission, if assumed to indicate the initial arrival of driver gas, show the correct behavior as the incident shock Mach number and the gas composition are varied (this will be demonstrated later). Hence, we will infer the time of the beginning of the arrival of significant driver gas contamination from the time of the sudden increase in light emission in the driven tube and nozzle. The arrival of the reflected driver rarefaction wave, another possible cause of the end of the test time, will be shown (Sec. IV.D) to occur at station E 1.2–1.25 ms after the initial shock wave, or well after the test time is already terminated due to driver gas contamination effects.

B. Measurements in Driven Tube, Station D

We first discuss the measurements of total light emission made at station D in the driven tube. Figure 2 shows experimental PMT light histories for run 24, with air in the driven tube, and for run 27, with N_2O/N_2 in the driven tube. The corresponding time histories from the pressure transducer located opposite the PMT are also shown in Fig. 2 with arbitrary origin and scale for the ordinate; here, these pressure histories are used only to determine the time at which the incident shock wave passes station D. The estimated times required for the uncontaminated driven tube gas to pass station D are indicated by arrows. The end of the uncontaminated test gas slug is assumed to pass by the PMT when the light emission increases roughly 5% of the height of the maxima seen when large quantities of driver gas pass by the PMT.

These estimates for the time required for the uncontaminated driven tube gas slug to pass by station D were successfully obtained for 24 of the 28 runs that were made with air or N_2O/N_2 in the driven tube. These optically inferred test times are plotted vs nozzle plenum enthalpy in Fig. 3. The error in determining these test times from the light data were judged to have a rather constant error band of

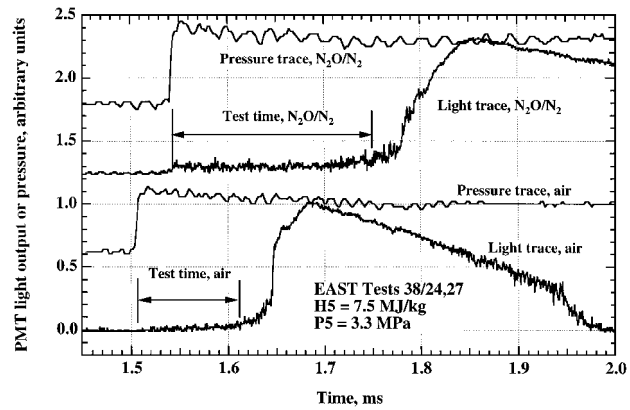

Fig. 2 Test times inferred from broadband light emission at station D in driven tube with upper light curve offset 1.25 for clarity; maximum light emission is roughly 1.0 for both curves. Pressure histories from the transducer at station D are also shown; for the pressure histories, both the origin and scale of the ordinate is arbitrary.

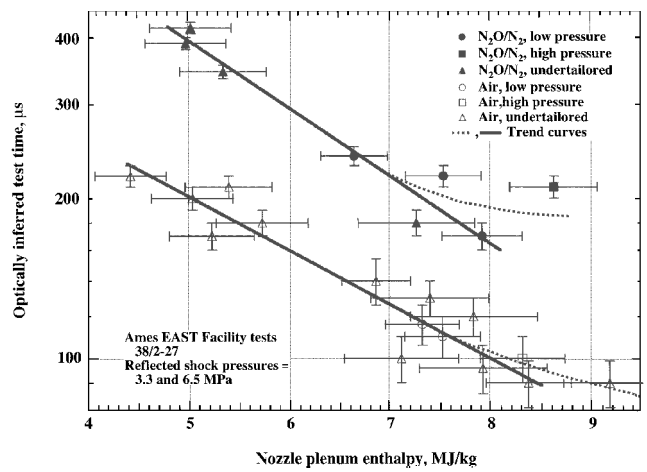

Fig. 3 Test times inferred from broadband light emission at station D in driven tube.

$\pm 10\ \mu$s, regardless of the size of the test time interval. This yields percentage error bands for the test times ranging from $\pm 10\%$ at test times of 100 μs down to $\pm 2.5\%$ at test times of 400 μs (as shown in Fig. 3). The nozzle plenum enthalpy was calculated from the extrapolated shock velocity at station E using the equilibrium incident and reflected shock calculation techniques of McBride and Gordon.[16] The plenum condition is achieved after the passage of the incident and reflected shocks. Shock velocities u_{BC}, u_{CD}, and u_{DE} were measured between stations B and C, stations C and D, and stations D and E, respectively. The error in the time interval defining u_{DE} obtained from the experimental data was $\pm 4\ \mu$s, leading to error bands of $\pm 1.0\%$ at shock velocities of 2.0 km/s increasing to 1.4% at velocities of 2.8 km/s. The velocity at station E (u_E) was obtained

by extrapolating from u_{DE} using the velocity drop from u_{CD} to u_{DE}. A second value of u_E was obtained by extrapolating from u_{DE} using the velocity drop from u_{BC} to u_{CD}. The difference between these two extrapolations to u_E was used as an estimate of the error in extrapolating from u_{DE} to u_E. The extrapolation error was found to be a maximum of $\pm$2.6% for runs 3–16 and a maximum of $\pm$1.5% for runs 17–29, after more experience had been gained in operating the facility. For runs 3–16, this leads to error band estimates of $\pm$4% for u_E and shock Mach number and $\pm$8% for the nozzle plenum enthalpy. For runs 17–29, the corresponding numbers are $\pm$2.5% and $\pm$5%. The corresponding error bars are shown in Fig. 3.

The open data points in Fig. 3 denote the data taken with air in the driven tube, and the solid data points denote data taken with N_2O/N_2 in the driven tube. For the moment, we will ignore the differences between triangle, square, and circle data points. For each set of data, straight trend lines have been drawn, which fit all data points well except the point at the highest enthalpy for each set. The trend lines flatten at high enthalpy, as shown by the dotted lines. Because there is only a single data point for each data set in the nonlinear region, we will consider only the solid, straight trend lines in the present discussion.

It is clear that the inferred test times at station D using N_2O/N_2 in the driven tube are consistently and substantially (60–100%) higher than those obtained with air in the driven tube. The observed increases in test time shown in Fig. 3 will now be compared with those predicted theoretically in Ref. 11. From the solid trend curves of Fig. 3, the percentage increases in test time obtained on substituting N_2O/N_2 for air in the driven tube were calculated for nozzle plenum enthalpies of 5, 6, 7, and 8 MJ/kg. These values are plotted as the open circles in Fig. 4. The procedure of dividing one experimental test time (for N_2O/N_2) by a second (for air) and subtracting unity to get the percentage increase can be shown to yield much larger error bands of $\pm$15 to $\pm$26%, which are shown for the open data points in Fig. 4. The theoretical curve from Ref. 11 is shown as the solid line. (The data points plotted as solid circles and squares will be discussed later.) It is seen that there is a reasonable agreement between the theoretically predicted and experimentally observed increases in test time.

With both air and N_2O/N_2 as the driven tube gas, the optically inferred test times discussed earlier were found to be between 0.39 and 0.51 times the theoretical values for a perfect plane interface between the driver and driven gas. There are a number of possible reasons for this 50–60% loss in test time, including boundary-layer buildup,[17] jetting of the driver gas as the main diaphragm opens,[18] curvature of the main diaphragm before rupture,[19] and instability and combustion at the interface.[8–10,20]

C. Measurements in the Nozzle, Station F

We now discuss light emission measurements made in the nozzle at station F. Some of the measurements were of broadband light emission into a PMT; others were made of emission at the argon 697-nm line using a monochromator. For runs 13–29, both types of measurements were made at station F. A detailed comparison of these histories showed that for each run, there was very little difference between the two light histories. It was concluded that the argon-specific radiation in the monochromator measurements was very likely overwhelmed by general broadband radiation. Hence, the light emission histories obtained from the monochromator at station F are regarded herein simply as a backup measurement of broadband light emission.

The increase in test time observed at station D in the driven tube upon changing from air to N_2O/N_2 did not carry over and appear as an increase in the time until driver gas arrival at station F for runs 1–16 and 20–22. Instead, a very much smaller increase in the time until driver gas arrival of 0–15% was observed. These runs were made at conditions that varied from significantly undertailored to slightly overtailored. Tailoring refers essentially to the relation between the acoustic impedance (i.e., the product of the density and the sound speed) of the driven tube gas, which has been compressed by the incident shock wave, and that of the expanded driver gas immediately behind the driven gas–driver gas interface. For two adjacent regions of ideal gas at the same pressure, the acoustic impedance can easily be shown to be proportional to $(\gamma\rho)^{0.5}$. Undertailored means that the driven tube gas has the higher $(\gamma\rho)^{0.5}$ value, whereas overtailored means the reverse. It can be argued that having a significantly overtailored condition, with the driver gas tending to be the denser gas, pushing the driven gas along, produces an interface between the gases that is more stable. With the interface being more stable, the mixing of the driven and driver gases would be reduced and the length of the driven gas slug would be greater and it would retain its identity farther down the driven tube. With this in mind, the facility operating conditions were shifted to operating substantially overtailored to attempt to find conditions under which test time increases due to substitution of N_2O/N_2 for air in the driven tube would persist beyond station D and into the nozzle.

Substantially overtailored conditions were selected for runs 17 and 18 and 23–28 in Table 2. The conditions for runs 17 and 18 were derived from those for runs 1–9 by reducing the driven tube fill pressure from 56–90 to 16.8–20.8 kPa, the driver conditions remaining unchanged. This leads to increased compression and heating of the driven tube gas and increased expansion and cooling of the driver gas, shifting the operating condition of the facility very strongly toward overtailored. Similarly, the conditions for runs 23–28 were derived from those for runs 10–16 mainly by dropping the driven tube fill pressure from 30–40 to 7.74–11.5 kPa.

We now proceed to examine light emission in the nozzle at station F for the overtailored runs 17 and 18 and 23–28. Figure 5 shows the light histories from the monochromator located at station F for run 24, with air in the driven tube, and for run 27, with N_2O/N_2 in the driven tube. The monochomator was tuned to the Ar 697-nm line. The optically inferred test times are taken to begin at the first abrupt light increase. This is due to the arrival of the first shock at station F and occurs at a time that was very consistent from run

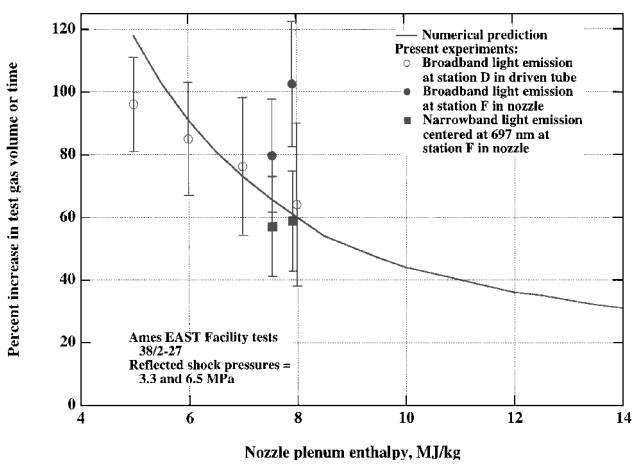

Fig. 4 Numerical and experimental values for the percentage increase in test gas volume or test time achieved by using N_2O/N_2 in the driven tube; error band for enthalpy is $\pm$5% for solid data points and $\pm$5 to $\pm$8% for open data points.

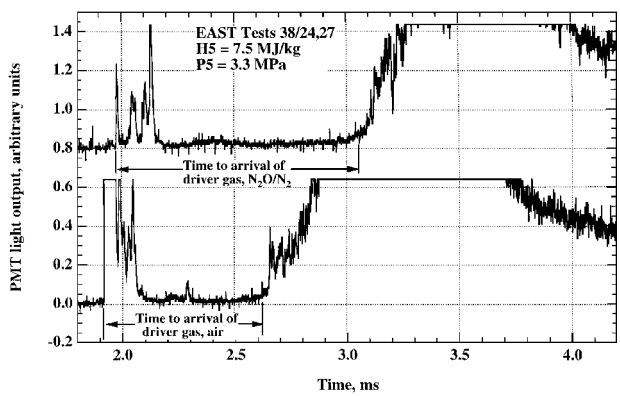

Fig. 5 Test times inferred from narrow-band light emission obtained using a monochromator centered at 697 nm; upper curve offset 0.8 for clarity and maximum light emission is roughly 1.0 for both curves.

to run. The later sharp emission peaks, which occur over a period extending about 200 μs after the first peak, are believed to involve light emission from burning secondary diaphragm material and were extremely inconsistent from run to run. The secondary diaphragm material, Kapton, can burn in the test gas, regardless of whether the initial driven tube gas was air or N_2O/N_2. For the first four runs, aluminum foil had been used for the secondary diaphragms. The burning of the aluminum foil produced much stronger light emission than the burning of the Kapton film, hence the change to Kapton.

The end of the uncontaminated test gas slug is assumed to pass by the monochromator when the PMT signal increases roughly 5% of the maximum reached when large quantities of driver gas pass by the monochromator (as was done in Sec. IV.B). These maxima cannot be seen in Fig. 5 because of saturation of the digitizers, but can be estimated from the shapes of the curves available in Fig. 5 and the shapes of the curves of similar data taken from early test runs at lower digitizer sensitivity. The heights of the maxima in Fig. 5, estimated in this way, are roughly 1.0. Using these techniques to define the optically inferred test times at station F, we can obtain the times until the arrival of driver gas indicated in Fig. 5. The estimated error band for these times is $\pm$5%.

Successful estimates of optically inferred times until driver gas arrival at station F in the nozzle were obtained for runs 17, 18, and 23–27. These optically inferred times until driver gas arrival are plotted vs nozzle plenum enthalpy in Fig. 6. The estimated error bands for enthalpy in Fig. 6 are $\pm$5%, following the analysis in Sec. IV.B. The open data points denote the data taken with air in the driven tube and the solid data points data taken with N_2O/N_2 in the driven tube. The data taken at higher pressures (in runs 17 and 18) are denoted by squares, the remaining data, taken at lower pressures, by circles. For all of these runs, both narrow-band monochromator and broadband emission measurements using a PMT were taken at station F. A graph corresponding to Fig. 6 was also prepared from the broadband PMT data; it only showed rather minor differences from Fig. 6 and, hence, is not presented here. It is seen that the optically inferred times until driver gas arrival at station F in the nozzle are roughly 60% greater with N_2O/N_2 in the driven tube than with air in the driven tube for runs 17, 18, and 23–27. Thus, for substantially overtailored facility operating conditions, the increase in test time (or time until driver gas arrival) found upon substituting N_2O/N_2 for air in the driven tube at station D in the driven tube was found to persist into the nozzle.

It is more difficult to establish the ratio of the test times (or times until driver gas arrival) for operation with N_2O/N_2 to those with air from the data of Fig. 6 than from the data of Fig. 3, because many fewer data points are available in the former case. It was decided not to use any extrapolations. Hence, a straight line was drawn, fit to the three air data points and, using this line and the two N_2O/N_2 data points at about 7.5 and 7.9 MJ/kg, ratios of times until driver gas arrival were constructed. These data points are the solid squares in Fig. 4. A similar procedure was used with the PMT broadband emission signal from station F in the nozzle (not presented herein) to yield the data points shown as solid circles in Fig. 4. Following the procedure given in Sec. IV.B for the estimate of error bands for the percentage increase in test time (or time until driver gas arrival), the error bands for the solid data points of Fig. 4 were estimated to vary from $\pm$16% at increases of 60% to $\pm$20% at increases of 100%. It is seen that three of the four estimates of increases in time until driver gas arrival obtained at station F upon substituting N_2O/N_2 for air in the driven tube are in reasonable agreement with both the experimental data obtained at station D in the driven tube and the theoretical curve taken from Ref. 11. One data point obtained from station F is about 67% higher than the other data points and the theoretical curve.

D. Pressure Measurements in the Nozzle Plenum, Station E

We now discuss pressure measurements made in the nozzle plenum at station E. As we have noted in Sec IV.C, the light emission measurements at station F in the nozzle indicated increases in the time until driver gas arrival obtained by substituting N_2O/N_2 for air in the driven tube only for the substantially overtailored facility operating conditions of runs 17, 18, and 23–28. The same effect was noted in regard to the pressure histories recorded at station E in the nozzle plenum. Only those pressure histories for these same overtailored test runs showed the test time increases upon changing from air to N_2O/N_2.

Experimental nozzle plenum pressure histories for runs 24 (with air) and 27 (with N_2O/N_2) are shown in Fig. 7 as the solid curves. Computational fluid dynamics (CFD) simulations are shown as dotted curves and will be discussed later. Before discussing the differences between operation with air and N_2O/N_2 in detail, we will describe the features seen in the N_2O/N_2 pressure history. (This history was chosen because, for this condition, it yielded a much better defined test time.) First, at about 1.86 ms, we see the incident shock wave. Next, there are two sharp pressure rises at about 1.91 and 1.94 ms. These are believed to be due to the passing of the two shock waves of the bifurcated foot of the reflected shock over the pressure transducer, and we present subsequently arguments to this effect. In Ref. 21, axisymmetric Navier–Stokes CFD solutions were obtained for the flow near the end of the driven tube in the NASA Ames Research Center EAST facility. CFD pressure histories were obtained at diagnostic station F, 2.54 cm upstream of the driven tube end wall and were compared with the corresponding experimental data. In Fig. 11 of Ref. 21, CFD and experimental pressure histories at station F are presented for a run with N_2 at 13.3 kPa pressure in the driven tube and a shock velocity of 1.49 km/s. The CFD and experimental times between the two pressure rises in question are 28.6 and 26.5 μs, respectively. Using the shock tube solver mode of the calculation package of Ref. 16, the reflected shock velocity for this facility operating condition was calculated to be 0.339 km/s. This leads to separations of the shock feet of 0.97 and 0.90 cm, respectively (for a transducer 2.54 cm from the end wall). From the expanded original data

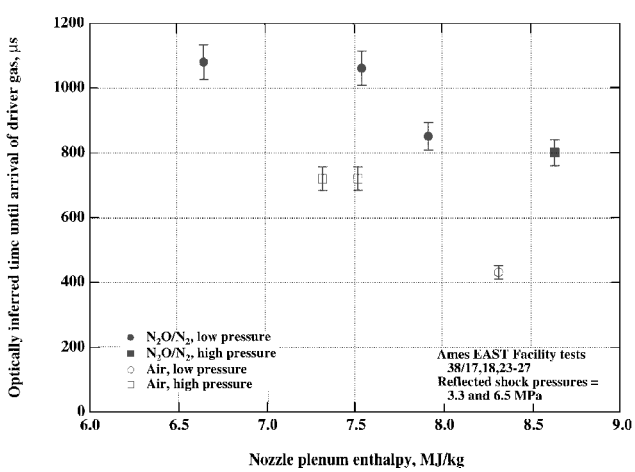

Fig. 6 Times until arrival of driver gas contamination inferred from narrow-band light emission centered at 697 nm in the nozzle at station F; error band for enthalpy is $\pm$5%.

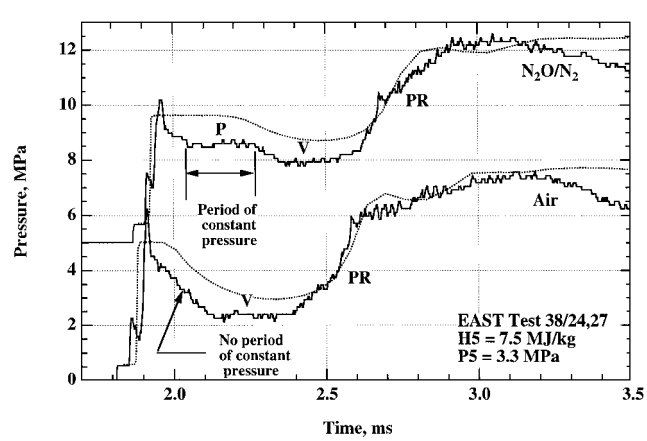

Fig. 7 Experimental (—) and CFD (. . .) pressure histories at nozzle entrance, where P denotes plateau region, V valley region, and PR the region of the steep pressure rise; the ordinate for N_2O/N_2 has been offset by 5 MPa for clarity.

traces of the data shown in Fig. 7, the times between the two pressure rises in question are 34 and 48 μs for the N_2O/N_2 and air test runs, respectively. The corresponding reflected shock velocities, calculated as already described, were 0.475 and 0.456 km/s. This leads to corresponding estimates of the separations of the shock feet of 1.61 and 2.19 cm. These are about twice as large as those implied by the pressure histories of Fig. 11 of Ref. 21 but are, perhaps, not unreasonable when compared to the contour plots of the CFD solution shown in Fig. 7 of Ref. 21 or the shadowgraphs of Figs. 3d–3f of Ref. 22.

Continuing along the pressure history, a relatively constant pressure period lasting about 240 μs is noted. Then the pressure drops about 20%, and a period of lower pressure lasting about 300 μs ensues, bringing us out to about 2.60 ms, after which the pressure starts to rise rapidly, reaching a maximum at about 3.10 ms. Thereafter, the pressure starts to fall due to the arrival of the reflected driver rarefaction wave. The general features described earlier, incident shock, two sharp pressure rises from the bifurcated reflected shock, drop to a relatively constant plateau pressure level, further drop to a valley region lasting of the order of 300 μs, followed finally by a large pressure rise to a maximum and a subsequent fall due to the reflected driver rarefaction wave, were, in essence, found for all of the test runs 17, 18, and 23–28. The caveats to this statement are that the plateau region appears to be absent for runs 23 and 24 with air in the driven tube and was sloped downward about 16% for run 25 with N_2O/N_2 in the driven tube.

The pressures in the plateau region, the valley region, and in the large, wide pressure peak observed after 2.6–2.7 ms in Fig. 7 are believed to represent the pressures produced by stopping the momentum of the onrushing pure driven tube gas followed by a mixture of driven and driver gas, followed finally by pure driver gas. This was investigated further using the one-dimensional inviscid CFD code of Ref. 11.

The condition of the driven gas was calculated from the extrapolated shock velocity at station E (see also Sec. IV.B) using the equilibrium incident shock calculation techniques of McBride and Gordon.[16] The driver gas behind the interface was assumed to have the same velocity and pressure as the driven gas slug and the same average molecular weight as the He/Ar mixture initially loaded into the driver. To obtain the gas temperature in the moving driver gas pushing the driven gas, the experimental pressure maxima seen in Fig. 7 are taken to represent the pressure produced by a hammer shock stopping the driver gas. With the pressure ratio across this hammer shock known, using the standard ideal gas shock relations, the temperature in front of the hammer shock can easily be calculated.

With the gas conditions on the two sides of the interface now known, it is assumed that the volume fraction of, say, the driven gas, varies linearly with distance in the mixed gas region. At each point in the mixed gas region, the two gases are assumed to undergo constant pressure mixing and to come to an equilibrium temperature and composition. The total amount of driven gas in this initial condition of the CFD model is set equal to the actual total mass of driven gas in the experiment. With this constraint, there is only one free parameter in the initial condition, the width of the mixed gas region. The CFD solution is started just before the incident shock hits the driven tube end wall.

When the first solutions were obtained for the conditions of run 27, it was immediately apparent that the valley pressure level was only slightly (about 2.5%) below the plateau pressure level, whereas in the experimental data the difference was about 20%. At this point, it is worth discussing why there is a valley at all in the CFD solution; in other words, why does the pressure not increase smoothly from the plateau region to the maximum pressure behind the hammer shock in the driver gas? The explanation involves the substantial differences in molecular weight, specific heat ratio, and temperature between the driver and driven gases in the driven tube. The specific heat of the shock-heated driven tube gas can be much greater than that of the monatomic driver gas. When the gases are mixed, e.g., in a one-to-one ratio, the molecular weight of the mixture will tend to be close to the average molecular weight, but the temperature of the mixture can be highly skewed toward that of the component with the larger specific heat, in this case, the hotter driven tube gas. For the first CFD solutions referred to earlier, the minimum mixed gas density was about 5% below the driven gas density, leading to the valley depth of about 2.5% already referred to. It was clear that the minimum mixed gas density must be much lower, as much as 30% below the driven gas density, to produce valleys in the CFD solutions that are as deep as those observed experimentally for the runs with N_2O/N_2, such as run 27.

A second possible cause of a density minimum is as follows. It is possible that the helium and argon loaded into the driver tube did not completely mix in the 1–2 h wait time before each run. When the electric discharge is struck and the main diaphragm breaks, this could lead to a low-density region of helium-enriched driver gas running out in front of the main helium-argon region of accelerated driver gas. A calculation of the density of the mixed gas zone was made with the mole fraction of helium in the driver gas varying linearly (with distance) from 0.667 at the driver end of the mixed gas zone to 1.0 at the driven end of the mixed gas zone. This produced a minimum mixed gas density 15% below the driven gas density; this minimum density is still very much too large to produce the experimentally observed valley depths.

A third possible cause of a density minimum is as follows. When the diaphragm first ruptures, the opening takes the form of two narrow, crossed slits.[23] During this phase of the flow, the driver gas pressure is 500–1000 times the driven gas pressure and the fine jets of driver gas can put a significant amount of driver gas into the region, which then acts as the driven tube when the diaphragm opens fully. For the present facility conditions, this driver gas in the driven tube region can initially have a static enthalpy three times the expected value for the ideal moving driver gas pushing the driven gas. This driver gas in the driven tube region will be compressed and heated further when the diaphragm opens fully, reaching static enthalpies as much as 5–15 times (with mixing and heat loss mechanisms neglected) the static enthalpy of the ideal moving driver gas pushing the driven gas. The quantity of driver gas undergoing this heating is substantial when compared to the quantity of driven gas. This mechanism provides, then, a very powerful means for heating the mixed gas zone and, hence, reducing its density. Some aspects of this process are discussed in Ref. 24.

It is assumed that the last mechanism described is responsible for a large increase in enthalpy and a large reduction in density in the mixed gas zone, i.e., sufficient density reduction to cause the experimentally observed valley depths. To model this enthalpy increase in the mixed gas zone, the following technique was used. The constant pressure mixing between driver and driven gas referred to earlier produces a given mixture static enthalpy at each point in the mixed gas region. To model the static enthalpy increase, the original static enthalpy at each point in the mixed gas zone is multiplied by $1 + R_h \sin[\pi(x - x_{mn})/(x_{mr} - x_{mn})]$, where R_h is the maximum enthalpy increase ratio and x is the axial position within the mixed gas zone. Thus, there is zero static enthalpy increase at the two ends of the mixed gas zone and a maximum static enthalpy increase ratio R_h at the center of the mixed gas zone. With this method of setting the initial condition for the CFD solutions, there are now two free parameters, the width of the mixed gas zone and the maximum static enthalpy increase ratio.

The two theoretical (CFD) pressure histories (shown in Fig. 7) were obtained by optimizing R_h and the width of the mixed gas zone to best model the two experimental histories. Before discussing the agreement between the theoretical and experimental pressure histories of Fig. 7, one should discuss what our one-dimensional, inviscid CFD calculations do not model. Clearly, our CFD calculations are incapable of modeling the two shock waves of the bifurcated shock foot and the overshoot phenomena seen in the two-dimensional Navier–Stokes solutions (e.g., Fig. 11 in Ref. 21), the experimental data therein, and the experimental data of Fig. 7. All of these phenomena are replaced by the single shock jumps seen in the CFD solutions of Fig. 7. Further, the pressure levels for the plateau and valley regions of the CFD solutions are about 20% higher than the corresponding levels of the experimental pressure histories. This is believed to be due to the lack of wall friction effects in the present inviscid CFD solutions. This will be discussed later. Finally, no attempt has been made to model the driver rarefaction in the present CFD solutions.

We now compare the experimental and theoretical pressure histories of Fig. 7. The CFD pressure histories were obtained by first

adjusting the enthalpy increase (R_h) to make the ratio between the CFD valley and plateau pressures equal to the experimentally observed values. Then, the width of the mixed gas zones was varied until the times of the drops from the plateau pressure to the valley pressure in the CFD solutions were in reasonable agreement with those observed experimentally. We note that the CFD solution for run 24 shows a short plateau region whereas the experimental data appear to show no plateau at all. It is possible that the plateau in the experimental pressure history exists but is obscured by the overshoot phenomenon seen, for example, in Fig. 11 of Ref. 21.

At this point, there are no free parameters remaining in the CFD solutions to allow one to set the time of the pressure rise from the valley to the maximum pressure behind the driver gas hammer shock. The times of these pressure rises are, nevertheless, rather well predicted by the CFD calculations. This is one reason that the authors believe that the CFD model constructed herein does model the actual process in the shock tube reasonably well. A second observation supporting the accuracy of the CFD modeling is as follows. For the two CFD solutions discussed, the ratios of the lengths of the pure driven gas zones ahead of the mixed gas zones to those expected if the interface was perfect (i.e., with no mixed gas zone) were 0.42 and 0.58 for the solutions for runs 24 and 27, respectively. From the experimental light emission data at station D in the driven tube (see Sec. IV.B), these corresponding ratios were estimated to be 0.41 and 0.45, respectively, in reasonably good agreement with those deduced from the experimental pressure measurements at station E using the CFD model.

We note that the maximum enthalpy increase ratios (R_h values) required to model the valley pressures correctly are very substantial, 0.548 for run 27 with N_2O/N_2 in the driven tube and 1.45 for run 24 with air in the driven tube. The driver conditions are identical for these two runs, but the mass of the gas in the driven tube for run 24 is only 0.67 that for run 27, leading one to expect a greater enthalpy increase ratio for the former case, as was found to be necessary to construct the best fitting CFD simulations.

We now study, in some detail, the pressure levels and durations of the experimental plateau and valley regions of the pressure histories at station E. The data from the pressure histories for runs 17,18, and 23–28 are shown in Fig. 8, normalized by the pressure in the reflected shock region calculated for pure driven tube gas from the shock velocity at station E. The abcissa is the calculated nozzle plenum enthalpy for pure driven tube gas. The error bands for the plenum enthalpy, calculated as discussed in Sec. IV.B, are $\pm$5%. The error bands for the calculated reflected shock pressure, which depends in the same way as the enthalpy on the shock velocity, are also $\pm$5%. The estimated accuracy of the experimental pressure measurements in the plateau and valley regions is $\pm$5%. Thus, the error bands for the pressure ratios, which appear in the ordinate of Fig. 8, are $\pm$10%, as shown. Each run provides, in general, two data points: the upper for the plateau pressure and the lower for the valley pressure. For the two low-pressure air runs, there were no easily distinguishable plateaus and, hence, there are no plateau data points in Fig. 8. (The air pressure history shown in Fig. 7 is from one of these runs.) Beside each upper (plateau) data point is given the duration of the plateau in multiples of 100 μs. One of the plateaus was rather significantly sloped downward; this is noted in Fig. 8.

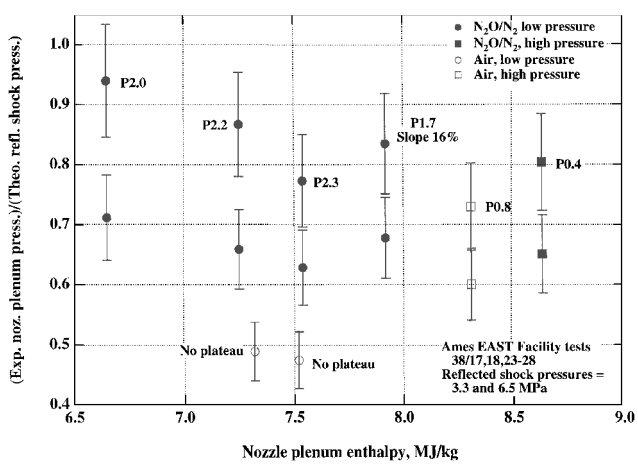

Fig. 8 Ratios of experimental nozzle plenum pressures to theoretical reflected shock pressures plotted vs nozzle plenum enthalpy and latter pressures calculated from the extrapolated shock velocities, where P are plateau pressure ratios and unannotated points valley pressure ratios; error band for enthalpy is $\pm$5%.

We note that the plateau pressures are not equal to the calculated reflected shock pressures, but, rather, range from $\sim$10% below the calculated value for enthalpies of $\sim$7 MJ/kg to $\sim$25% below the calculated value for enthalpies of $\sim$8.5 MJ/kg. This is believed to be due to wall friction effects acting between the time the shock wave passes station E (for which time the theoretical pressures are calculated) and the time range of the plateau region. Once the shock wave reflects, one no longer has a simple shock wave continuously slowing down as it progresses along a tube. For this reason, the authors did not believe it was justified to perform a further extrapolation of the decreasing shock velocity beyond station E to attempt to improve the agreement between the calculated reflected shock pressures and the measured plateau pressures.

For the six low-pressure runs (runs 23–28), there is a large, consistent difference between the data with air and N_2O/N_2 in the driven tube. All four runs with N_2O/N_2 have a plateau, which lasts $\sim$200 μs. One of these plateaus is sloped somewhat, as is noted in Fig. 8. The upper pressure history of Fig. 7 is representative of the data for these runs. The two runs with air in the driven tube are very similar in shape to each other and do not show any easily distinguishable plateau regions. One of these pressure histories is shown as the lower history in Fig. 7. We also note that the valley pressures are much lower (47–49% of the calculated reflected shock values) with air in the driven tube than with N_2O/N_2 in the tube (63–71% of the calculated reflected shock values).

This description is completely consistent with there being a much shorter slug of pure driven gas for the cases with air in the driven tube and is strongly supported by the CFD simulations for run 24 (which also models run 23) and run 27 (which also models run 28) discussed earlier. Further, runs 25 and 26 differ from runs 27 and 28 only in the driven tube fill pressure (respectively, 7.74, 11.5, 9.21, and 9.21 kPa) and, thus, the CFD model for run 27 roughly models runs 25 and 26 as well.

We turn briefly to the two runs at the higher reflected shock pressure level of $\sim$65 bar. These data are inconclusive. The pressure levels shown in Fig. 8 indicate a slightly better performance using N_2O/N_2 in the driven tube. However, the duration of the plateau, albeit at a lower pressure level, is greater with air in the driven tube.

E. Estimates of Lengths of Slugs of Compressed Driven Tube Gas

Estimates were made, using three different techniques, of the lengths of the compressed slug of pure driven gas at the nozzle entrance. The first technique is as follows. The reflected shock velocity at the end of the driven tube and the sound speed in the doubly compressed pure driven tube gas can be estimated reasonably accurately given the incident shock velocity. The estimates of these two velocities are assumed to have the same error band width as the shock velocity, that is, $\pm$2.5% (see Sec. IV.B). The time of passage of the reflected shock past the pressure transducer at station E is taken as the mean of the times of the two peaks in the pressure history indicating the passage of the two shocks of the bifurcated foot of the reflected shock (see Sec. IV.D and Fig. 7). The time of arrival, at the transducer, of the head of the expansion wave produced by the reflected shock wave leaving the region of pure driven gas and entering the region of mixed driver plus driven gases with variable density (and variable acoustic impedance) is taken to be the time at the end of the plateau period of the pressure history. (The error bands of the difference between these two times was judged from the data to be $\pm$5% for the longest time intervals, increasing to $\pm$18% for the shortest intervals.) From these data and the known position of the transducer, the length of the gas slug can readily be calculated. The errors discussed earlier are summed up to give error bandwidths for the slug lengths varying from $\pm$7.5 to $\pm$20.5%.

A second technique starts with the measurements made (Sec. IV.B) of the time taken for the singly compressed pure driven gas slug to pass by station D in the driven tube. The error band of this time measurement varies from $\pm$4% for the longest intervals (240 ms)

Table 4 Estimated test gas slug lengths at nozzle entrance

Run number	Driven tube gas	Driven tube gas pressure, torr	Shock velocity at E, km/s	Nozzle plenum enthalpy, MJ/kg	Slug l, cm (from pressure histories at E)	Slug l, cm (from light histories at D)	Slug l, cm (from light histories at F)
17	Air	126	2.81	8.31	8.0 ± 1.6	6.0 ± 0.8	0.38 ± 0.03
18	N_2O/N_2	156	2.69	8.63	5.4 ± 0.9	10.8 ± 0.8	1.02 ± 0.08
23	Air	58	2.65	7.32	<2.5	6.6 ± 0.7	0.77 ± 0.06
24	Air	58	2.68	7.52	<2.5	6.1 ± 0.7	0.78 ± 0.06
25	N_2O/N_2	58	2.57	7.92	13.8 ± 1.4	8.5 ± 0.7	1.05 ± 0.08
26	N_2O/N_2	86	2.34	6.65	11.0 ± 0.8	10.8 ± 0.7	1.07 ± 0.08
27	N_2O/N_2	69	2.51	7.54	10.6 ± 1.0	10.6 ± 0.7	1.28 ± 0.10
28	N_2O/N_2	69	2.45	7.25	10.0 ± 1.0	13.9 ± 1.0	—

to $\pm$10% for the shortest time intervals (see Sec. IV.B). The length of this slug can readily be calculated from the time interval and the gas slug velocity calculated from the shock velocity (with an error band of $\pm$2.5%; see Sec. IV.B). This length is then increased by 18.6% to allow for the additional driven tube length between station D and the tube endwall. Finally, it is then decreased by the expected density ratio across the reflected shock wave. The error bandwidths already given are summed up to give total error bandwidths for the slug lengths ranging from $\pm$6.5 to $\pm$12.5%.

The third technique starts with the measurements of the times to arrival of driver gas contamination inferred from light emission histories taken at station F in the nozzle (Sec. IV.C, error bandwidth estimated to be $\pm$5%). The sound speed and specific heat ratio at the nozzle plenum gas conditions can be estimated reasonably accurately from the measurements of incident shock velocity. The error bandwidth of the estimated sound velocity is taken to be equal to that of the incident shock velocity, i.e., $\pm$2.5% (as given in Sec. IV.B). With these parameters available and knowing the nozzle throat diameter, the length of the pure driven gas slug required to drain through the nozzle in the observed optically inferred test time can readily be calculated. The total error bandwidth is taken to be the sum of those error bandwidths given earlier, or $\pm$7.5%. Table 4 lists the slug lengths calculated by these three different techniques for runs 17, 18, and 23–28. The error bands for the shock velocities and the plenum enthalpies are $\pm$2.5 and $\pm$5%, respectively (as given in Sec. IV.B).

Of the 23 estimates of the test gas slug length, 21 show the substantial superiority of N_2O/N_2 over air as the driven tube gas. The only exceptions are the two estimates made from the pressure histories at station E for runs 17 and 18. These are the same two data sets that produced the inconclusive results discussed at the very end of Sec. IV.D.

We see from Table 4 that the estimated slug lengths at the nozzle entrance as calculated from the pressure histories at station E and the light emission histories at station D are within a factor of 1.6 of each other for five runs, differ by a factor of 2 for one run and differ by a factor of $\sim$2.5 or, possibly, more for two runs (runs 23 and 24). In general, considering the difficulty of the measurements and the number of assumptions made to calculate the slug lengths, the authors regard these results as reasonably consistent with each other.

Turning to the slug lengths calculated from the light emission histories at station F, we see that these values are 5–10 times less than the corresponding values calculated from the data at stations D and E for six of the eight runs. Even for runs 23 and 24, this ratio may be as large as $\sim$3. It is clear that the interface between the pure driven tube gas and the mixed gas initially established 2.5–13 cm upstream of the nozzle entrance spreads and deteriorates rapidly as the test gas is flowing through the nozzle. Presumably, this is related to the jets of driver gas seen driving into the driven gas in the CFD solutions of Ref. 21. In other words, the arrival of driver gas at station F in the nozzle is not determined by the drainage time for a pure driven gas slug bounded on the upstream edge by a nearly planar interface, but rather by the time it takes the driver gas jets to penetrate sufficiently far into the driven gas slug to reach the nozzle entrance.

The pressure histories at station E for tests 23 and 24 could, at first glance (see, for example, the lower history of Fig. 7) be taken to indicate zero test time with pure driven gas, inasmuch as the length of the plateau region appears to be zero for these cases. However, even with the assumption of zero plateau length, these pressure histories do not exclude the existence of a pure driven gas slug in the 2.54 cm between the transducer and the nozzle entrance. This is why in column 6 of Table 4 for these runs, we see the entry <2.5 cm. Hence, these two pressure histories at station E are not inconsistent with the slug lengths of $\sim$0.78 cm estimated from the light histories at station F for these runs.

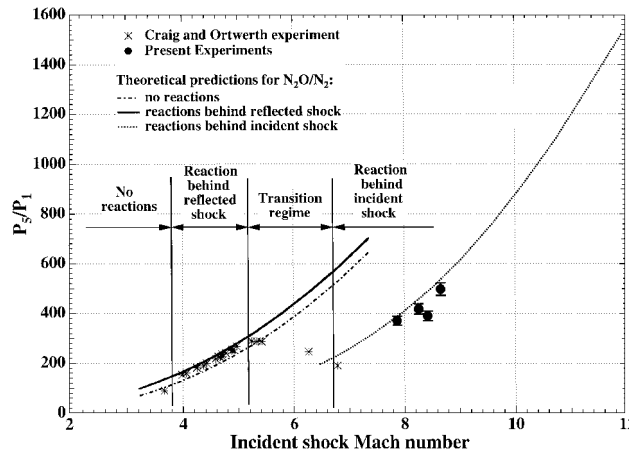

Fig. 9 Ratios of pressure behind reflected shock to initial driven tube fill pressure vs incident shock Mach number; error band for Mach number for present data is $\pm$2.5%.

F. Reflected Shock Pressure Ratios

In Ref. 13, Craig and Ortwerth present experimental measurements of the ratio of the pressure behind the reflected shock to the initial driven tube fill pressure for shock tube operation with N_2O/N_2 in the driven tube. Data were given for initial shock Mach numbers up to 6.8. The data were compared to theoretical predictions with no chemical reactions taking place, with chemical reactions behind the reflected shock, and with chemical reactions behind the initial shock. It was demonstrated that as the shock Mach number increased, the data shifted from matching the theoretical curve with no chemical reactions to matching the theoretical curve with chemical reactions at the reflected shock to, finally, matching the theoretical curve with chemical reactions at the incident shock. Only a single datum of Ref. 13 fits the theoretical curve with reactions at the incident shock. The theoretical pressure ratio curves of Ref. 13 were extended by Wilson et al.[11]

The plateau pressure levels of shots 25–28, which were discussed in Sec. IV.D, yield four additional experimental reflected shock pressure ratios, obtained at shock Mach numbers above those investigated in Ref. 13. The error bandwidths for the shock Mach numbers are $\pm$2.5% (see Sec. IV.B), and experimental plateau pressures are estimated to have error bandwidths of $\pm$5%. Figure 9 shows the experimental reflected shock pressure ratio data of Craig and Ortwerth[13] (star data points) compared with the three theoretical curves with no chemical reactions, chemical reactions at the reflected shock, and chemical reactions on the incident shock. As already mentioned, the maximum incident shock Mach number for the experimental data of Craig and Ortwerth[13] is 6.8. The four data points from the present investigation are shown as the solid circle data points in Fig. 9. These data are in reasonably good agreement with the theoretical curve and extend the range of the experimental data to incident shock Mach numbers of 8.7. The new experimental

data points are 5–20% below the theoretical curve, likely because of the frictional effects discussed in Sec. IV.D in connection with the data of Fig. 8.

Summary and Conclusions

An experimental investigation was carried out into the replacement of air in the driven tube of a reflected shock tunnel by N_2O/N_2 in order to increase the test time. The work was done in the 10-cm-diam EAST at the NASA Ames Research Center. A series of 29 runs were made, 17 with air in the driven tube, 10 with N_2O/N_2 in the driven tube, and 1 with Ar in the driven tube. (All data were lost in one run.) The pressures behind the reflected shock were either $\sim$3.3 or $\sim$6.5 MPa, and the incident shock velocities ranged between 2 and 3 km/s, corresponding to nozzle plenum enthalpies of 4–9 MJ/kg. Test times were estimated from light emission histories in the driven tube (at about 84% of the way to the nozzle inlet) and in the nozzle at an area ratio of 27.9 and from pressure histories just upstream of the nozzle entrance.

The test times estimated from the light histories in the driven tube showed that consistent increases of 60–100% were obtained upon substituting N_2O/N_2 for air in the driven tube. These increases were in very good agreement with theoretical estimates. All test times (with either driven tube gas) were about 40–50% of the ideal values expected with a perfect interface between the driver and driven gases.

The times of driver gas arrival estimated from the light emission histories in the nozzle did not show significant improvements with N_2O/N_2 for cases where the facility was operated between significantly undertailored to slightly overtailored conditions. They did show substantial improvements with N_2O/N_2 when the facility was operated at substantially overtailored conditions. It is believed that this may be due to the greater stability of the driver–driven interface at overtailored operating conditions. At overtailored operating conditions, increases in the time until driver gas arrival of 60–100% with N_2O/N_2 were observed, which were in reasonable agreement with the theoretical estimates.

The test times estimated from the pressure histories at the nozzle inlet followed, for the most part, the trends of those estimated from the light emission histories in the nozzle. Substantial improvements in test time with N_2O/N_2 were observed only when the facility was operated at substantially overtailored conditions. The six runs made at the lower reflected shock pressure ($\sim$3.3 MPa) showed a consistent, large increase in test time with N_2O/N_2. The two runs at the higher reflected shock pressure of $\sim$6.5 MPa were inconclusive.

During operation of the facility, a slug of test gas is created just upstream of the nozzle entrance. This slug has been compressed by both the incident and reflected shock waves. Lengths of the slug were estimated from all three types of data discussed. All of the slug length estimates made from the light emission data in the driven tube showed a substantial superiority of N_2O/N_2 over air in the driven tube. (Typical length increases were 60–100%.) These slug lengths were all about 40–50% of those that would be expected for a perfect driver–driven gas interface. Of the 25 estimates made of slug lengths for operation at substantially overtailored conditions, 23 showed a similar substantial superiority of N_2O/N_2 over air in the driven tube. Only the pressure data at the nozzle inlet for two runs was inconclusive in this regard.

The slug lengths estimated from the driven tube light emission histories were roughly in agreement with those estimated from the nozzle inlet pressure histories. The slug lengths estimated from the light emission histories in the nozzle, assuming drainage of a pure driven gas slug through the nozzle, were typically 3–10 times less than those estimated by the other techniques. Thus, the arrival of driver gas contamination in the nozzle does not seem to follow from simple drainage of a well-behaved test gas slug through the nozzle, but rather, from the arrival of jets of driver gas in the driven tube at the nozzle inlet.

Reflected shock pressure ratios measured with N_2O/N_2 in the driven tube for the substantially overtailored condition were found to compare reasonably well with theoretical predictions. Previous experimental data was limited to a maximum incident shock Mach number of 6.8. The present results extend the Mach number range up to a maximum of 8.7.

Acknowledgments

Support by NASA (Contract NAS-2-14031) to Eloret is gratefully acknowledged. The excellent support of the NASA Ames Research Center EAST facility crew, R. J. Exberger and R. E. Warren, was very important for this research effort.

References

[1]Cavolowsky, J. A., Loomis, M. P., Bogdanoff, D. W., Zambrana, H. A., Newfield, M. E., and Tam, T. C., "Flow Characterization in the NASA Ames 16-Inch Shock Tunnel," AIAA Paper 92-3810, July 1992.

[2]Deiwert, G. S., Cavolowsky, J. A., and Loomis, M. P., "Large Scale Scramjet Testing in the Ames 16-Inch Shock Tunnel," AIAA Paper 94-2519, June 1994.

[3]Eitelberg, G., McIntryre, T. J., Beck, W. H., and Lacey, J., "The High Enthalpy Shock Tunnel in Göttingen," AIAA Paper 92-3942, July 1992.

[4]Eitelberg, G., "First Results of Calibration and Use of the HEG," AIAA Paper 94-2525, June 1994.

[5]"Description of the Aachen Shock Tunnel TH2," Shock Wave Lab., Technical Univ., Aachen, Germany, Jan. 1991.

[6]"Hypersonic Shock Tunnel—Description and Capabilities," Calspan Corp., Buffalo, NY, Jan. 1987.

[7]Hornung, H. G., "Performance Data of the New Free-Piston Shock Tunnel at GALCIT," AIAA Paper 92-3943, July 1992.

[8]Harris, C. J., Marston, C. H., Rogers, D. A., Mallin, J. R., and Warren, W. R., "A High Density Shock Tunnel Augmented by a Faraday MHD Accelerator," *Fourth Hypervelocity Techniques Symposium*, Arnold Engineering Development Center, Tullahoma, TN, 1965, pp. 234–273.

[9]Copper, J. A., Miller, H. R., and Hameetman, F. J., "Correlation of Uncontaminated Test Durations in Shock Tunnels," *Fourth Hypervelocity Techniques Symposium*, Arnold Engineering Development Center, Tullahoma, TN, 1965, pp. 274–310.

[10]Bird, K. D., Martin, J. F., and Bell, T. J., "Recent Developments in the Use of the Hypersonic Shock Tunnel as a Research and Development Facility," *Third Hypervelocity Techniques Symposium* (Denver, CO), 1964, pp. 7–50.

[11]Wilson, G. J., Sussman, M. A., and Loomis, M. P., "The Use of Nitrous Oxide to Increase Test Times in High Enthalpy Shock Tunnels," AIAA Paper 94-2597, June 1994.

[12]Wilson, G. J., "Time Dependent Quasi-One Dimensional Simulations of High Enthalpy Pulse Facilities," AIAA Paper 92-5096, Dec. 1992.

[13]Craig, R. R., and Ortwerth, P. J., "Use of Nitrous Oxide for Obtaining High Stagnation Enthalpies in Shock Tunnels," *AIAA Journal*, Vol. 5, No. 12, 1967, pp. 2271–2274.

[14]Sharma, S. P., and Park, C., "Operating Characteristics of a 60- and 10-cm Electric Arc-Driven Shock Tube—Part I: The Driver," *Journal of Thermophysics and Heat Transfer*, Vol. 4, No. 3, 1990, pp. 259–265.

[15]Sharma, S. P., and Park, C., "Operating Characteristics of a 60- and 10-cm Electric Arc-Driven Shock Tube—Part II: The Driven Section," *Journal of Thermophysics and Heat Transfer*, Vol. 4, No. 3, 1990, pp. 266–272.

[16]McBride, B. J., and Gordon, S., "Computer Program for Calculation of Complex Chemical Equilibrium Compositions and Applications: II. Users Manual and Program Description," NASA Reference Publication 1331, June 1996.

[17]Mirels, H., "Shock Tube Test Time Limitation Due to Turbulent-Wall Boundary Layer," *AIAA Journal*, Vol. 2, No. 1, 1964, pp. 84–93.

[18]Cambier, J.-L., Tokarcik, S., and Prabhu, D. K., "Numerical Simulations of Unsteady Flow in a Hypersonic Shock Tunnel Facility," AIAA Paper 92-4029, July 1992.

[19]Daru, V., and Damion, J. P., "Analysis of the Flow Perturbations in a Shock Tube Due to the Curvature of the Diaphragm," 19th International Symposium on Shock Waves, Marseille, France, July, 1993.

[20]Flagg, R. F., "Advances in Shock Tunnel Driving Techniques," *Third Hypervelocity Techniques Symposium* (Denver, CO), 1964, pp. 7–50.

[21]Wilson, G. J., Sharma, S. P., and Gillespie, W. D., "Time-Dependent Simulations of Reflected-Shock/Boundary-Layer Interaction," AIAA Paper 93-0480, Jan. 1993.

[22]Takano, Y., Miyoshi, S., and Akamatsu, T., "Reflection Processes of Ionizing Shocks in Argon on an End Wall of a Shock Tube," *Proceedings of the 12th International Symposium on Shock Tubes and Waves* (Jerusalem, Israel), Magnes Press, Hebrew Univ., Jerusalem, Israel, 1979, pp. 187–196.

[23]Cheng, D. Y., Dannenberg, D. E., and Stephens, W. E., "A Novel Use of a Telescope to Photograph Metal Diaphragm Openings," *AIAA Journal*, Vol. 7, No. 6, 1969, pp. 1209–1211.

[24]Zeitoum, D., Brun, R., and Valetta, M.-J., "Shock-Tube Calculations Including the Diaphragm and Boundary-Layer Effects," *Proceedings of the 12th International Symposium on Shock Tubes and Waves* (Jerusalem, Israel), Magnes Press, Hebrew Univ., Jerusalem, Israel, 1979, pp. 180–186.

W. Oberkampf
Associate Editor